Chemosphere 256 (2020) 127141

Contents lists available at ScienceDirect

Chemosphere

journal homepage: www.elsevier.com/locate/chemosphere

Extracellular electron transfer leading to the biological mediated production of reduced graphene oxide

Yue Lu [a, b, *], Linrui Zhong [a, b], Lin Tang [a, b, **], Huan Wang [a, b], Zhaohui Yang [a, b], Qingqing Xie [a, b], Haopeng Feng [a, b], Meiying Jia [a, b], Changzheng Fan [a, b]

[a] College of Environmental Science and Engineering, Hunan University, Changsha, 410082, China
[b] Key Laboratory of Environmental Biology and Pollution Control (Hunan University), Ministry of Education, Changsha, 410082, Hunan, China

HIGHLIGHTS

- Provided a green chemistry strategy for the biological production of reduced graphene oxide (RGO) by *Geobacter*.
- Bacterially induced RGO by *Geobacter* exhibited a good performance in electrochemical conductivity.
- The doping of nitrogen and phosphorus elements were observed in the bacterially induced RGO by *Geobacter*.
- Extracellular electron transfer at microbial cell/GO interface promoted the graphene oxide (GO) reduction of *Geobacter*.

GRAPHICAL ABSTRACT

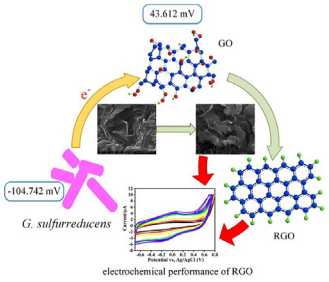

ARTICLE INFO

Article history:
Received 3 November 2019
Received in revised form
26 March 2020
Accepted 19 May 2020
Available online 21 May 2020

Handling Editor: Chang-Ping Yu

Keywords:
Geobacter
Reduced graphene oxide
GO reduction
Extracellular electron transfer

ABSTRACT

To explore a green, low-cost, and efficient strategy to synthesis reduced graphene oxide (RGO), the process and mechanism of the graphene oxide (GO) reduction by a model electrochemically active bacteria (EAB), *Geobacter sulfurreducens* PCA, were studied. In this work, up to 1.0 mg mL^{-1} of GO was reduced by *G. sulfurreducens* within 0.5–8 days. I_D/I_G ratio in reduced product was similar to chemically RGO. After microbial reduction, the peak which corresponded to the reflection of graphene oxide (001) disappeared, while another peak considered as graphite spacing (002) appeared. The peak intensity of typical oxygen function groups, such as carboxyl C–O and >O (epoxide) groups, diminished in bacterially induced RGO comparing to initial GO. Besides, we observed the doping of nitrogen and phosphorus elements in bacterially induced RGO. In a good agreement with that, better electrochemical performance was noticed after GO reduction. As confirmed with differential pulse voltammetry (DPV) and cyclic voltammetry (CV) analysis, the maximum value of peak currents of bacterially induced RGO were significantly higher than those of GO. Our results showed the electron transfer at microbial cell/GO interface promoted the GO reduction, suggesting a broader application of EAB in biological mediated production of RGO.

* Corresponding author. College of Environmental Science and Engineering, Hunan University, Changsha 410082, China.
** Corresponding author. College of Environmental Science and Engineering, Hunan University, Changsha 410082, China.
E-mail addresses: yuelu@hnu.edu.cn (Y. Lu), tanglin@hnu.edu.cn (L. Tang).

https://doi.org/10.1016/j.chemosphere.2020.127141
0045-6535/

1. Introduction

Due to its unique properties, graphene has been used in a wide spectrum of applications such as energy-storage, catalysis and sensors (Li et al., 2008b; Mohanty and Berry, 2008; Kauffmanab and Star, 2010; Karim et al., 2013; Wei et al., 2015). However, common chemical approaches employed to reduce graphene oxide (GO) to graphene require high temperature and suitable reactors with hazardous chemicals involved (Stankovich et al., 2007; Li et al., 2008a; Wang et al., 2009, 2012; Zhou et al., 2009), which may cause serious economic or environmental concerns (Wang et al., 2011).

Microbial reduction of GO first explored by Salas et al. (2010) is considered as a green chemistry approach to produce reduced graphene oxide (RGO) (Bansal et al., 2015). Previous studies reported that several bacterial groups were capable to perform GO reduction, such as *Escherichia coli* (Gurunathan et al., 2013), *Shewanella* (Salas et al., 2010), *Gluconobacter roseus* (Rathinam et al., 2018), and other microbial species (Mokkapati et al., 2018; Manasi. et al., 2018; Combarros et al., 2016; Bansal et al., 2015). The known mechanism of microbial reduction of GO driven by metabolically generated electrons can be largely divided into two modes: i) direct electron transfer through direct contact of GO with surface-associated proteins, and ii) indirect electron transfer via self-secreted redox electron mediators by electrochemically active bacteria (EAB) (Akhavan and Ghaderi, 2012; Zhao et al., 2018). For example, *Shewanella* sp., an important model of EAB, was able to reduce GO with the participation of self-secreted redox electron mediators, e.g., electron shuttle(s) (Wang et al., 2011) and cytochromes MtrCAB/OmcA/CymA (Salas et al., 2010; Jiao et al., 2011; Wang et al., 2011). Shen et al. (2018) investigated two types of self-assembled bio-rGO-hydrogels produced via GO reduction in the presence of *Shewanella* sp. *(S. xiamenensis*, *S. putrefaciens* and *S. oneidensis*). In their study, bio-rGO hydrogels and *Shewanella* together showed a good performance on Congo red decolorization and hexavalent chromium bioreduction, while sole *Shewanella* could not fulfill.

Similar to *Shewanella, Geobacter* as another model EAB was able to apply extracellular substance as electron acceptors and coupled it to organic compounds oxidation (Logan, 2009; Liu et al., 2017). *Geobacter sulfurreducens* were reported to utilize various extracellular substances (e.g. Fe(III)) for respiration in order to obtain energy for growth (Lovley et al., 1993; Mahadevan et al., 2006), and their mechanisms for extracellular electron transport could be attributed to c-type cytochromes (c-Cyts) and nanowires as well as the cell-secreted redox molecules (Okamoto et al., 2014; Kalathil et al., 2019). As reported, *G.sulfurreducens* PCA contained a large number of genes coding for c-Cyts (111 in the whole genome) (Busalmen et al., 2008; Kalathil et al., 2019), and the detected electronic conductivity of its nanowires was ~5 mS cm^{-1}, which was equivalent to that of synthetic metal nanostructures (Malvankar et al., 2011). Besides, *Geobacter* was considered to get invovled in GO reduction. Kalathil et al. (2019) reported the oxygen evolution reaction catalyst was derived from GO reduction by *Geobacter*, and the hybrid catalyst (i.e., rGO/*Geobacter*) showed high electrocatalytic activity. Besides, Chen et al. (2018) investigated GO reduction in soil samples collected from a realgar tailing mine, in which the abundance of *Geobacter* increased after the addition of GO. However, the mechanism of GO reduction by *Geobacter* has not been fully addressed.

Therefore, *Geobacter* as another model EAB with strong extracellular electron transfer capability was selected to study its mechanism for GO reduction in order to further expand our knowledge of GO reduction via microbial route. Our results showed an effective reduction of GO to RGO by *G.sulfurreducens* PCA, and the bacterially induced RGO was further investegated by electrochemical test, transmission electron microscope (TEM), scanning electron microscopy (SEM), fourier transform infrared spectroscopy (FTIR), X-ray photoelectron spectroscopy (XPS), X-ray diffraction (XRD), Raman and Ultraviolet−visible spectroscopy (UV−vis). In the end, the putative mechanism of extracellular electron transfer at *G.sulfurreducens*/GO interface was proposed.

2. Marterials and methods

2.1. Cultivation of G. sulfurreducens

G. sulfurreducens was obtained from the research group of Prof. Hanqing Yu (University of Science & Technology of China). *G. sulfurreducens* was grown in modified DMSZ medium with 20 mM acetate as electron donor and 50 mM fumarate as electron acceptor at 30 °C (Li et al., 2014; Zhou et al., 2019). The medium in sealed serum vial kept an anaerobic atmosphere by N_2:CO_2 (4:1) mixed gas. The growth curve was detected by optical density measurement at 600 nm.

2.2. Biosynthesis of RGO

Single layer GO was purchased from XFNANO, INC, China. 100 mg of GO powder was dissolved in 50 mL sterile distilled water by sonicating for 3 h, which was stored in 4 °C as main stock. 20 mM acetate and calculated volume of the GO stock were added to the bacterial medium as electron donor and acceptor, respectively, to reach the final concentration of GO as 0.1, 0.2, 0.4, 0.6, 0.8, 1.0 mg mL^{-1}, respectively. A 5% inoculum of strain PCA in exponential growth phase (Fig. S1) was transferred into GO-amended medium (20 mL) and all the cultures were statically cultivated in the 30 °C incubator. Control treatment was set up in the GO-amended medium without the addition of strain PCA. Sampling tests were conducted on Day 9, when the GO reduction induced by *G. sulfurreducens* PCA was observed for all GO treatments. RGO which was produced in 0.6 mg mL^{-1} GO-amended medium, was investigated by Raman, XRD, UV−vis, FTIR and XPS analysis. Each treatment was performed in quadruplicate.

2.3. Characterization

Electrochemical measurements were studied in a three-electrode system to investigate the electrochemical activity of *G. sulfurreducens*, in which RGO and GO with a glassy carbon electrode (GCE) as working electrode, a saturated calomel electrode (SCE) as reference, and a Pt wire as counter electrode. Open circuit voltage (OCV), cyclic voltammetry (CV) (range from −0.7 V to 0.8 V, scan rate 1 mV/s) and Differential pulse voltammetry (DPV) (range from −0.6 V to 0.4 V, potential increment: 0.004 V; amplitude: 0.05 V; pulse width: 0.2 s; pulse period: 0.5 s) were collected using a CHI760E electrochemical workstation (Shanghai Chenhua Instrument Co., Ltd., China). *G. sulfurreducens* cells and RGO were collected via centrifugation at 5000 and 8500 rpm for 5 min respectively, and then washed three times with PBS (0.2720 g L^{-1} KH_2PO_4, 0.2840 g L^{-1} Na_2HPO_4, pH 7.0) (You et al., 2018). The harvested RGO resuspended with Nafion (7.5 μL RGO precipitation + 2.5 μL 0.05% Nafion). The acquisition of resuspended GO was the same as RGO. 5 μL of *G. sulfurreducens* cells, resuspended GO or resuspended RGO were drop casted over the GCE, then quickly dried by a blower (cold air) until the surface forming a film for electrochemical measurements (You et al., 2018). Nitrogen saturated solution and room temperature were kept during electrochemical test. The electrochemical data of each sample were collected in triplicate.

The steps of removing cell debris were as follows. All the RGO samples were gathered via centrifugation at 8500 rpm for 5 min and further washed in ultrapure water, 80% ethanol and 1 M HCl (Salas et al., 2010). The samples were then freeze-dried and stored for characterization.

Surface elemental components of the RGO and GO were determined with a Thermo ESCALAB 250XI XPS (Thermo Fisher Scientific, America). The crystal structures were determined with XRD using a X' Pert PRO MPD diffractometer (Holland Panalytical, Holland) with Cu Kα (1.5406 A) radiation. FTIR transmission spectra of the materials were obtained using a Bruker Vertex 70 FTIR (Bruker, America). Raman spectra were recorded using a LabRAM HR800 Raman spectrometer (Horiba Jobin Yvon, France) with an exciting wavelength of 514.6 nm argon laser. The morphology of RGO was analyzed with TEM and SEM. UV–vis spectra of the aqueous suspension of RGO and GO were obtained using a TU-1901 UV-VIS spectrometer (Beijing Purkinje General Instrument Co., Ltd, China).

3. Results and discussion

3.1. GO reduction by G. sulfurreducens

After adding *G. sulfurreducens* to GO treatments, black particle aggregation was observed as shown in Fig. 1, which might due to the decrease of polar functionalities on the edges of reduced material with the increase of its hydrophobicity (Rathinam et al., 2018). Reduction of GO was observed in all the treatments in the presence of *G. sulfurreducens*, while visible form change was not observed in the control, a treatment without adding strain PCA (Fig. S2). In this study, the color change and formation of black particle aggregation were observed in the medium amended with 0.1, 0.2, 0.4, 0.6, 0.8, and 1.0 mg mL^{-1} GO after 0.5, 1, 2, 3, 5, and 8 d of cultivation, respectively (Fig. 1 and S2), which indicated the reduction of GO and the production of suspended graphene that appeared black and insoluble (Gurunathan et al., 2013). Average time consumed for the formation of RGO via microbial reduction of GO by *G. sulfurreducens* was shorter than that of most GO-reducing bacteria (Gurunathan et al., 2013; Yoshida et al., 2016; Chen et al., 2018; Shen et al., 2018). For example, *E. coli* was capable to reduce 0.5 mg mL^{-1} of GO to RGO after Day 3 (Gurunathan et al., 2013), and the reduction of 0.17 mg mL^{-1} GO and production of RGO were observed in the presence of *Shewanella* (*S. xiamenensis* BC01, *S. oneidensis* MR-1 and *S. putrefaciens* CN32) after two days of cultivation (Shen et al., 2018).

Exhaustive microscopic inspection on the morphology of nanomaterials with microbes was researched through TEM and SEM in this study. *G. sulfurreducens* was enveloped or partial wrapped within materials films (Fig. 2c and g), and the curly surface of reduced materials might due to the decreased hydrophobicity of the sheets edge and internal stayed hydrophilic (Shen et al., 2018). In comparison with pure *G. sulfurreducens* treatment (Fig. 2a and e), the bacterial cells in the treatments amended with low concentration of GO (0.1–0.6 mg mL^{-1}) kept intact membrane and no particles of nanomaterial was found from the interior of *G. sulfurreducens* cells (Fig. 2c and g). Even though the membrane of most cells remained intact, the damaged cell membrane in high GO amendments (>0.8 mg mL^{-1}) was observed (Fig. S3), suggesting the toxicity of GO/RGO to *G. sulfurreducens* might be dose-dependent (Wang et al., 2019b). GO was considered as a carbon nanomaterial with good biocompatibility, which was able to enhance the cell proliferation, and RGO was reported as an inhibitor for bacterial growth (Akhavan and Ghaderi, 2012; Gurunathan et al., 2013; Combarros et al., 2016; Ren et al., 2018). While in this study, the weaker toxicity and affinity of RGO comparing to GO nanowalls might due to partial removal of oxygen functionalities on their surface after GO reduction (Hu et al., 2010; Hu and Zhou, 2013). Therefore, bacterial toxicity of GO and RGO were not fully addressed. Besides, bacteria harbored the intracellular enzyme like dehydrogenase, which was able to deoxidate a small amount of GO that entered the cells (Wang et al., 2019b). These results suggested that reduction of GO by gram-negative *G. sulfurreducens* was mainly an extracellular process, however, partial of GO/RGO entered the *G. sulfurreducens* cells in the treatments amended with high GO concentration and an intracellular GO reduction process might occur.

3.2. Characterizations of GO and RGO

SEM and TEM images of GO showed pristine GO had a flat and smooth thin-layered structure with few creases (Fig. 2b and f). While the surface of RGO reduced by *G. sulfurreducens* became thick, corrugated and wrinkled, therefore their 2D membrane structure could keep thermodynamically stable (Fig. 2d and h) (Wang et al., 2012).

Raman scattering, a tool to characterize disorder in carbon material was applied in this study to monitor the GO reduction process (Prakash and Bahadur, 2014; Chen et al., 2016; Tang et al., 2018b). Raman spectra of GO exhibited a strong G peak at ~1609 cm^{-1} and a strong D peak at ~1359 cm^{-1} (Fig. 3d). The G and D peaks appeared due to the first order scattering of the E_{2g} phonon (the doubly degenerate in-plane optical vibration) of sp^2 carbon atoms and breathing mode of the A_{1g} symmetry (the molecule M is completely symmetrical with an one of the lattice sites as center), respectively (Gurunathan et al., 2013; Reich and Thomsen, 2004). While in RGO, these two peaks shifted to a lower wavenumber at ~1604 cm^{-1} and ~1352 cm^{-1}, respectively (Fig. 3c and d), which indicated the damage of sp^2 network and the formation of defects in RGO (Gurunathan et al., 2013). The I_D/I_G (the idensity ratio of D and G bands) of GO was 0.945, while the I_D/I_G fraction of RGO was 1.324 (Fig. 3c and d). The increase of I_D/I_G in RGO compared with pristine GO was caused by the removal of oxygen function groups, indicating the disorder and the number of sp^2 cluster increased after reduction (Prakash and Bahadur, 2014; Zhao et al., 2018). Ratio I_D/I_G of RGO reduced by *G. sulfurreducens* was higher than that of most synthetic RGO (including one-step solvothermal route, bio-synthesized graphene and laser reducing GO) as summarized in Table S1. Additionally, similar Raman spectra was observed in RGO with bacterial debris (Fig. 3b), however the ratio I_D/I_G slightly decreased from 1.380 to 1.324 after removal of bacterial debris, which might due to the reaction of remaining oxygen function groups of RGO with 80% ethanol in the washing step (Bansal et al., 2015). Besides, a peak at ~792 cm^{-1} indicated the presence of microbes was observed in the Raman spectrum of pure *G. sulfurreducens* and RGO with *G. sulfurreducens* (Fig. 3a and b), but it disappeared in the RGO samples after removal of bacterial debris, suggesting the microbes were completely removed.

FTIR analysis was performed to study the oxygen functional groups in GO and RGO as shown in Fig. 4. The peaks of aromatic C=C and C–H stretch were discovered at ~1639 and ~2922 cm^{-1}, respectively, and their peak intensity was similar in both GO and RGO. While values of four characteristic peaks in initial GO were higher than those of RGO, which were ~3437/3408, ~1398, ~1273 and ~1072 cm^{-1}, corresponding to O–H stretching, carboxyl C–O, C–O stretching, >O (epoxide), respectively. Those results indicated an obvious reduction in the peak intensity of various oxygen functionalities after GO reduction, such as hydroxyl, carboxyl, and epoxide functionalities (Chen et al., 2016; Cho et al., 2018; Zhou et al., 2019). FTIR of RGO reduced by *G. sulfurreducens* in this study was in a good agreement with other bacterially induced RGO

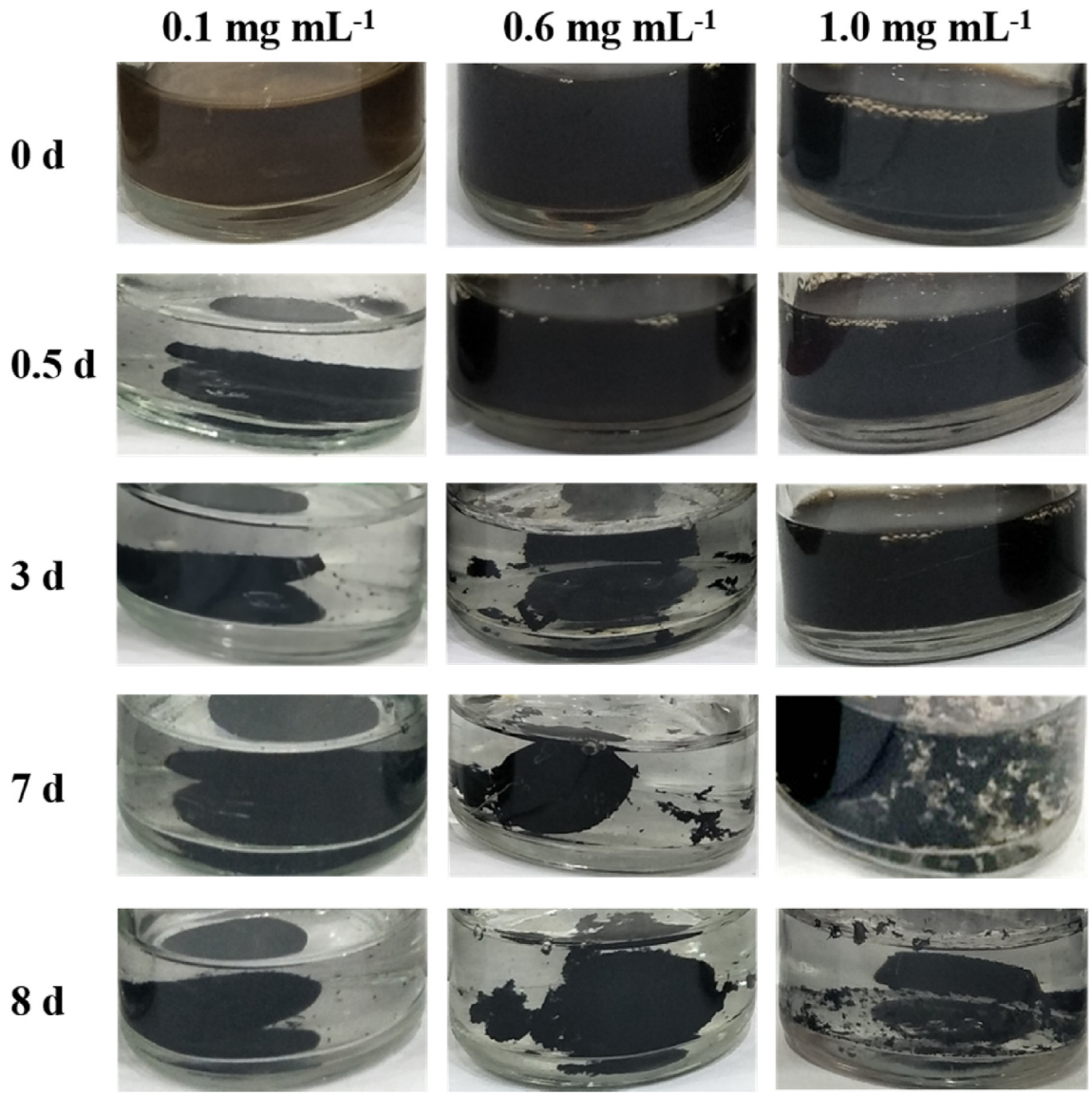

Fig. 1. The formation of RGO in the treatments with *G. sulfurreducens* and different initial concentration of GO (0.1, 0.6 and 1.0 mg mL^{-1}, respectively).

like those produced by *P. aeruginosa* PA01 and *S. xiamenensis* BC01 (Mokkapati et al., 2018; Shen et al., 2018). Two diffraction peaks at ~1350 cm^{-1} and ~1197 cm^{-1} corresponded to P—C bonds and $\nu_{p\text{-}o\text{-}c}$ (stretching vibration between P, O and C), respectively, were emerged after GO reduction, and approximate peaks were observed in porous graphene-black phosphorus nanocomposite (Cai et al., 2019). Additionally, the characteristic absorption peak at ~1168 cm^{-1} was detected in RGO corresponded to the CH_3(N) stretching and CH_2(N) stretching (Huang et al., 2018), suggesting RGO reduced by *G. sulfurreducens* contained N and P.

The elemental status and contents of C, O, N and P were determined by XPS spectroscopy as shown in Fig. 5. Compared with GO, XPS survey spectra of RGO performed extremely weak O 1s peak, and strong N 1s and P 2p peaks (Feng et al., 2018; Rajpurohit et al., 2019). The dominant XPS C 1s peaks of GO and RGO performed at approximately 284.6 eV, and the dominant XPS O 1s peaks of GO and RGO located at approximately 532 eV (Peng et al., 2018). An obvious decrease in the O/C ratio from 1.21 of GO to 0.49 of RGO was observed, which indicated the drop of corresponded oxygen functionalities for RGO (Fig. 5a and b). It reported that the O/C fraction for the hydrazine reduced GO varied from 0.21 to 0.09 with the increase dosage of hydrazine and the contact time (Bansal et al., 2015; Pei and Cheng, 2012). The peaks centered at ~284.8, ~285.2, ~286.9, ~288.9 and ~284.8 eV, could be respectively assigned to C—C, C—O/C═N, C═O/C—N, O—C═O and C—P (Fig. 5c and d) (Wang et al., 2019a). The post-reduction peak intensities for O—C═O and C═O were declined to a great extent, and the C—O peak of RGO was slightly increased, which indicated considerable deoxidation of GO in the presence *G. sulfurreducens*. The peak intensity post-reduction was increased at ~284.8 eV, showing the restoration of sp^2 bonded carbon after reduction. In addition, Fig. 5 (a) and (b) showed two additional peaks at ~400.1 and ~134.1 eV, indicating the RGO reduced by *G. sulfurreducens* contained N and P, respectively. The peaks at ~132.9, ~133.9, ~399.8, ~401.6, ~402.6, and ~398.9 eV were assigned to C—P, O═P, pyrrolic N, graphitic N, N—O, and pyridinic N, respectively (Fig. 5g and h and S4) (Tang et al., 2018a; Rajpurohit et al., 2019; Wang et al., 2019a). The N configuration in RGO was mainly consist of pyrrolic N (89.69%) and graphitic N (6.36%), which was well in agreement with the prepared N-doped graphene by implanting N_2 plasma (Wang et al., 2019a). N—O which was the N

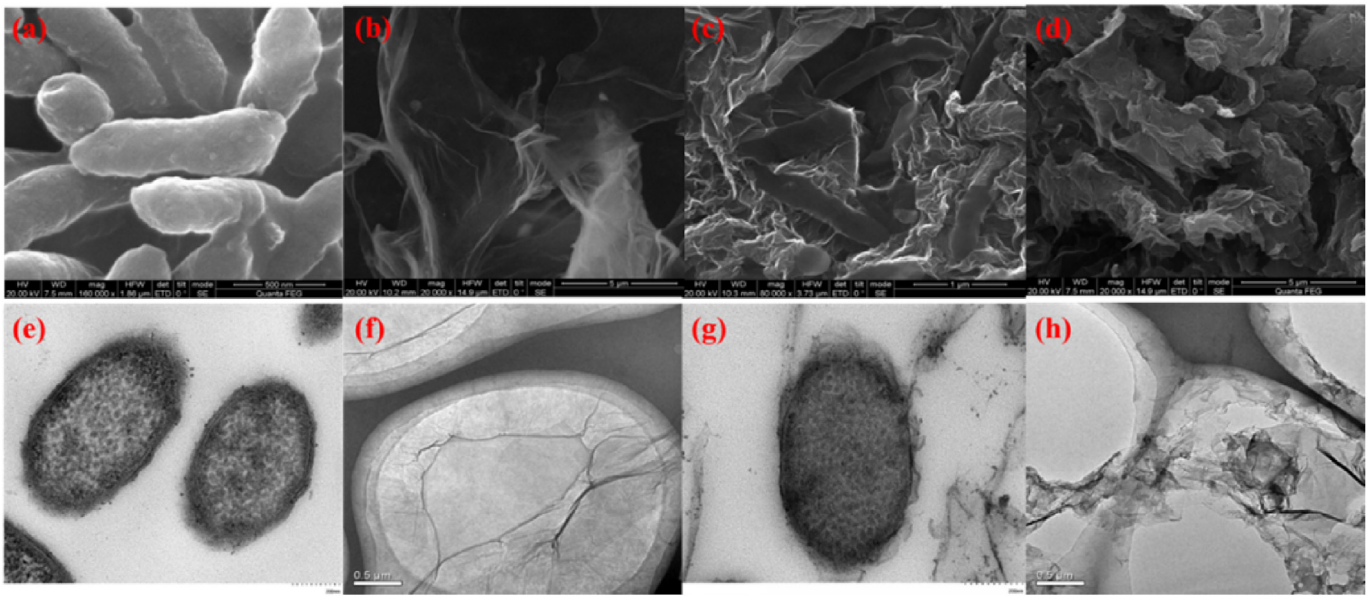

Fig. 2. SEM images of (a) pure *G. sulfurreducens*, (b) GO, (c) *G. sulfurreducens* cells with RGO, and (d) RGO after removal of *G. sulfurreducens* cells. TEM images of (e) pure *G. sulfurreducens*, (f) GO, (g) *G. sulfurreducens* cells with RGO, and (h) RGO after removal of *G. sulfurreducens* cells.

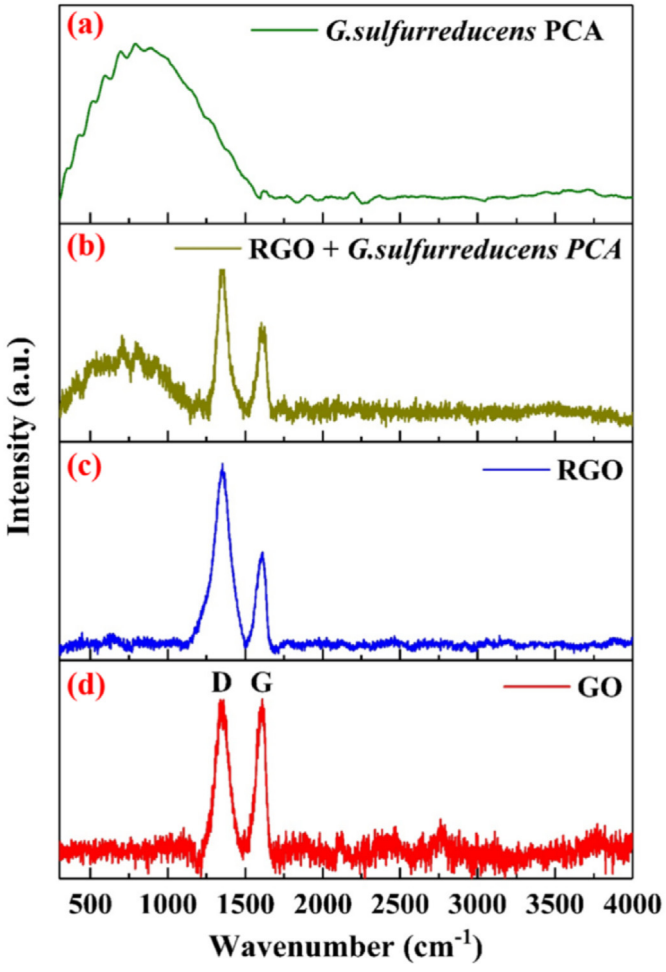

Fig. 3. Raman spectra of (a) pure *G. sulfurreducens* cells, (b) RGO with *G. sulfurreducens* cells, (c) RGO after removal of *G. sulfurreducens* cells, and (d) GO.

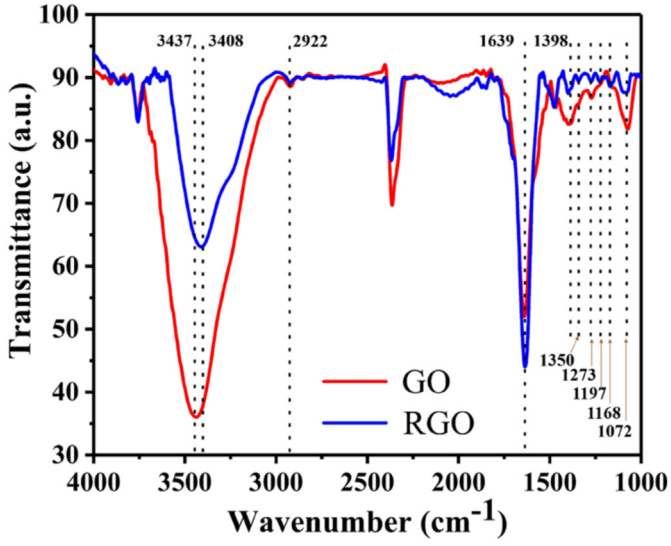

Fig. 4. FTIR spectra of GO and RGO reduced by *G. sulfurreducens*.

atom bonds with one O atom and two C atoms disappeared in RGO, which further indicated the decrease of the O content after reduction (Wang et al., 2019a). An increase of the N and P components in RGO indicated GO might chemically react with phospholipid or other biological macromolecules in *G. sulfurreducens* cell membrane (Figs. 4 and 5). As reported by Luan et al. (2015) GO was capable to interact with the free amine terminals of the enzymes.

The XRD spectra of GO and RGO were performed in Fig. S5. The GO exhibited an intense peak at 10.55° corresponded to the reflection of graphene oxide (001). After *G. sulfurreducens* reduction of RGO, the peak at 10.55° disappeared, and wide and intense diffraction peak at 28.12° appeared, which was considered as graphite spacing (002) according to previous study (Xu et al., 2011). The alteration of XRD spectra was likely caused by the change of interlayer spacing, the loss of oxygen functionalities and ordering of

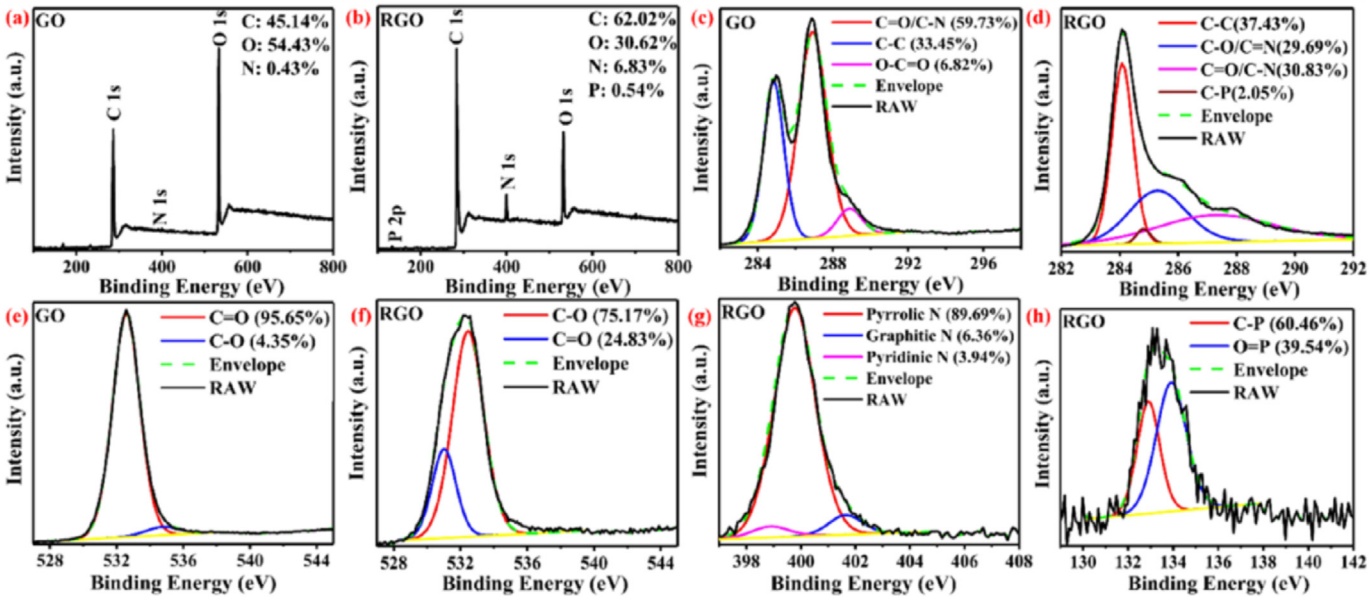

Fig. 5. XPS surveys of (a) GO and (b) RGO reduced by *G. sulfurreducens*. XPS C 1s spectra of (c) GO and (d) RGO reduced by *G. sulfurreducens*. XPS O 1s spectra of (e) GO and (f) RGO reduced by *G. sulfurreducens*. (g) XPS N 1s spectra of RGO reduced by *G. sulfurreducens*. (h) XPS P 2p spectra of RGO reduced by *G. sulfurreducens*.

the 2D structure (Xu et al., 2011; Zhao et al., 2018). The UV–vis analysis of GO showed a peak at 230 nm corresponded to π–π* electronic transitions of C–C and C=C bonds, while this peak was redshifted to 194 nm in RGO, which indicated the electronic conjugation restored (Fig. S6) (Williams and Kamat, 2009; Prakash and Bahadur, 2014; Cho et al., 2018). Besides, another peak observed in RGO at 254 nm corresponded to defects and vacancies indicated an increase of defect intensity (Cho et al., 2018). In summary, the characterizations analysis showed an effective decrease of oxygen function groups in reduced product, which indicated a significant reduction of GO to RGO.

3.3. Electrochemical characterization measurement of pure *G. sulfurreducens* and GO reduced by *G. sulfurreducens*

DPV of the test matrixes which performed the electrochemical activity of bacterial-culture constituents, including (i) 'Blank', the treatment with all required components in microbial culture except adding *G. sulfurreducens*, and (ii) 'Supernatant', the remaining medium after the removal of bacterial debris (Fig. 6a).

The reduction peak at 252 mV was observed in 'Supernatant' but not in 'Blank' (Fig. 6a), indicated that *G. sulfurreducens* could secrete some electrochemically active substances such as riboflavin or flavinmononucleotide (FMN) outside the cell, which could indirectly transfer electrons to extracellular electron acceptor (Okamoto et al., 2014). DPV results of *G. sulfurreducens* exhibited the reduction peak at −326 mV and the oxidation peaks at both −360 and −164 mV, due to various redox active c-Cyts in the membrane of *G. sulfurreducens* (Peng and Zhang, 2017; Cai et al., 2018). C-Cyts played important roles in the bacterial process of extracellular electron transfer. For example, OmcZ could directly transfer electrons through the biofilm, and OmcB was involved in the electron transfer across the extracellular electron acceptors/biofilm interface (Richter et al., 2009).

DPV showed the oxidation and reduction peak currents of RGO were in the range of 2.56 to 11.17 μA at −28 mV, and −2.40 to −10.95 μA at −158 mV, respectively (Fig. 7a). Besides, the anodic and cathodic peak currents of RGO were 1.24-4.36 and 1.24-5.64 times higher than those of GO, respectively, suggesting the improvement of electrochemical activity in RGO with the increase of initial concentrations of amended GO. Better performance in electrochemical activity of RGO was further confirmed by CV analysis (Fig. S7a). The anodic and cathodic peak currents of RGO were 1.05-2.31 and 4.69-18.77 times higher than those of GO in CV analysis, respectively, which was mainly due to the functional groups (e.g. O–C=O and C=O) in GO hindered the electron transfer between electrolyte and electrode surface leading to the decrease of electrochemical activity (Rostamabadi and Heydari-Bafrooei, 2019). Besides, the increase of N and P content in RGO and reduction of oxygen functionalities led to the increased current response of RGO comparing to initial GO (Rostamabadi and Heydari-Bafrooei, 2019; Wang et al., 2019a). The current values of RGO were similar to the chemically synthesized reduced graphene oxide (Afzali et al., 2019; Srivastava et al., 2019). For example, chemical reduced GO (e.g. with 0.1 M NaOH solution and 30 mg of sodium citrate) was ~10 μA (Afzali et al., 2019). Besides, Srivastava et al. (2019) modified a glassy carbon electrode (GCE) with rGO@WS_2QD_S in the presence of up to 84.2 μM of chloroquine, and detected current was lower than 6 μA by DPV.

DPV analysis of GO-amended medium, after the removal of bacterial debris and RGO, showed similar results in 'Supernatant' samples (Figs. 6a and 7b). In particular, the cathodic peak at 252 mV was observed only in the treatments of 0.6, 0.8, and 1.0 mg mL^{-1} of GO, which suggested higher concentration of GO amendment in *G. sulfurreducen* could promote the secretion of electrochemically active substances (e.g. riboflavin) outside the cell (Okamoto et al., 2014). However, further increase the initial GO amendment to 0.8 and 1.0 mg mL^{-1}, a clear decrease in cathodic peak currents of GO-amended medium was observed, which indicated the excessive dosage of GO might inhibit the growth of *G. sulfurreducens* and these results were in good agreement with the damaged cell membrane observed in TEM images (Fig. S3). Therefore, in this study 0.6 mg mL^{-1} of GO was considered as an optimal condition for *G. sulfurreducens* to perform GO reduction and the biosynthetic RGO had a desired electrochemical conductivity.

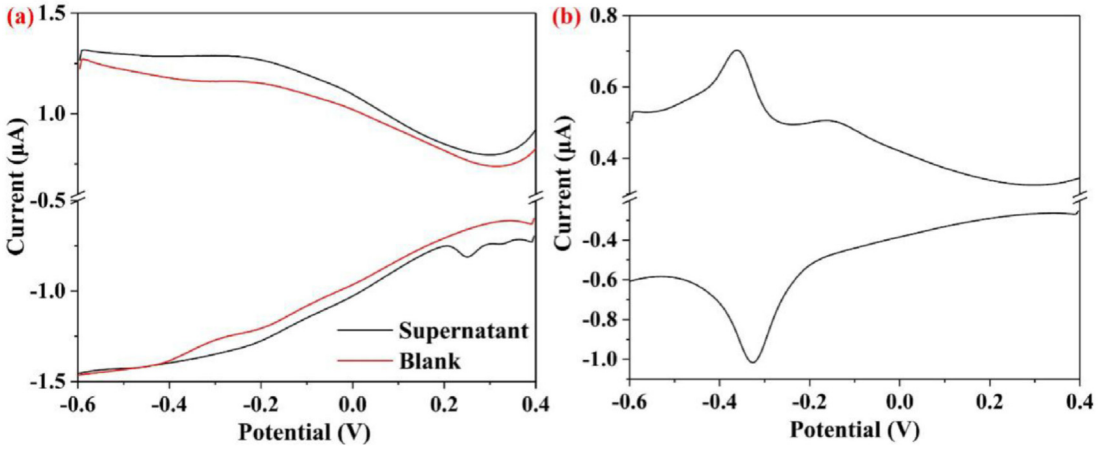

Fig. 6. DPV curve of (a) 'Blank'——a treatment with all required components except adding *G. sulfurreducens* and 'Supernatant'——the remaining bacterial medium after the removal of *G. sulfurreducens* and (b) pure *G. sulfurreducens*. (scan rate 1 mV/s, nitrogen saturated solution, room temperature, vs. SCE).

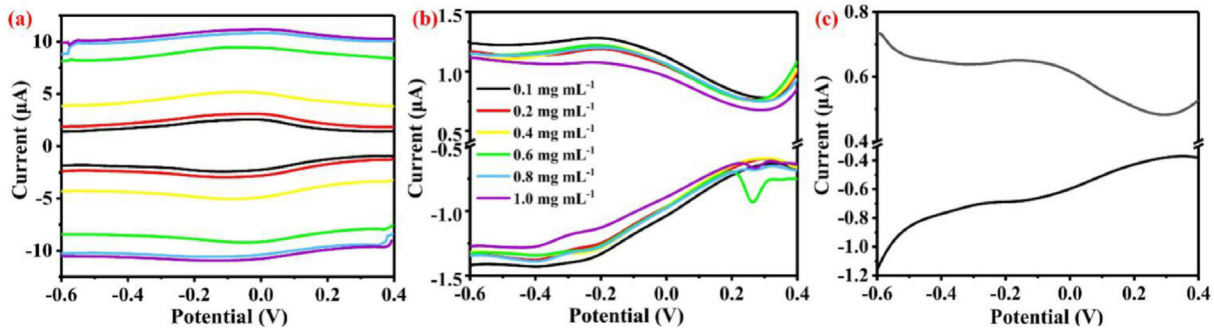

Fig. 7. DPV of (a) RGO reduced by *G. sulfurreducens*, (b) GO-amended medium after removal of RGO and *G. sulfurreducens*, and (c) GO (nitrogen saturated solution, room temperature, potential increment: 0.004 V; amplitude: 0.05 V; pulse width: 0.2 s; pulse period: 0.5 s, vs. SCE).

3.4. Possible mechanism for reaction of GO with G. sulfurreducens

To further probe possible mechanism for GO reduction by *G. sulfurreducens*, OCV of *G. sulfurreducens* and GO were detected. OCV of *G. sulfurreducens* was −104.142 mV, indicating that *G. sulfurreducens* surface had reducibility; while that of GO was 43.612 mV, indicating that GO surface was oxidative. Therefore, GO reduction by *G. sulfurreducens* was an oxidation-reduction reaction with electrons transferred from *G. sulfurreducens* to GO.

On the basis of our knowledge and available references of extracellular electron transfer pathway of *Geobacter*, putative metabolic interaction between GO and *G. sulfurreducens* was proposed in the Fig. 8. Acetate, as an organic substrate and electron donor, could enter the TCA cycle for NAD(P)H generation (Mahadevan et al., 2006; Meng et al., 2013). Electrons were shifted into the inner membrane by NAD(P)H dehydrogenase, then transferred out of the inner membrane by c-Cyts, and finally transported to the extracellular environment via outer membrane c-Cyts such as OmcB and OmcZ (Lovley, 2006; Meng et al., 2013; Song et al., 2016). Additionally, redox electron mediators such as riboflavin and FMN were generated and transferred outside the cell (Okamoto et al., 2014). Riboflavin or FMN secreted by *G. sulfurreducens* firstly bounded c-Cyts to transfer electrons instead of relying on riboflavin or FMN themselves (Michelson et al., 2017). Thus, self-secreted soluble redox electron mediators and c-Cyts were both involved in the electron transfer in the bacterial cells/GO interface of *Geobacter* (Michelson et al., 2017). However, the mechanism of GO reduction by *G. sulfurreducens* was different comparing to another conductive bacteria *Shewanella* (Jiao et al., 2011; Wang et al., 2011; Gurunathan et al., 2013). In our study, GO reduction of *G. sulfurreducens* mainly depended on the outer membrane c-Cyts especially in the treatments with lower GO amendments (<0.4 mg mL^{-1}), while GO reduction of *Shewanella* relied on both c-Cyts and flavin under the similar conditions (Wang et al., 2011; Delgado et al., 2019). Still, the types and functions of c-Cyts involved in the GO reduction of *G. sulfurreducens* were not fully addressed, and further identities of the key self-secreted electron mediators were required.

4. Conclusions

This study provided a green chemistry route for the biological production of RGO by *G. sulfurreducens*. These results confirmed that 0.6 mg mL^{-1} was an optimum dosage for *G. sulfurreducens* to perform GO reduction and the biosynthetic RGO showed a desired electrochemical conductivity. Higher amount of GO amendment caused the damage to the cell membrane. The mechanism for GO reduction by *G. sulfurreducens* was mainly through extracellular electron transfer at microbial cell/GO interface, while, further researches on the regulation of extracellular electron transport through c-Cyts as well as the key electron mediators in bacterially induced GO reduction are required. Overall, these results give further insight into the microbial reduction of GO by *G. sulfurreducens*, which provides a feasible method in the bioengineering and commercial application of functional bacteria in the production of graphene and its derivatives.

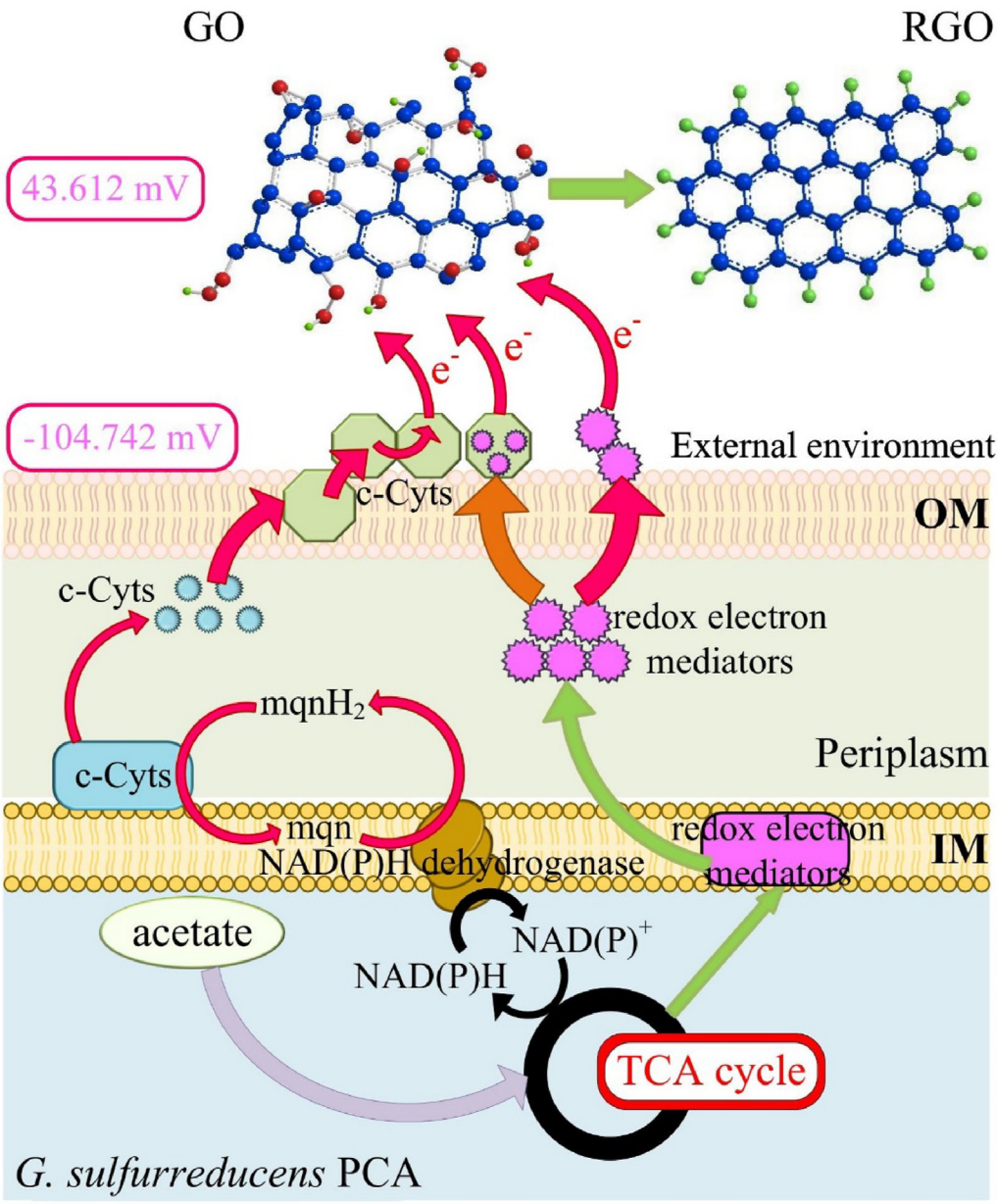

Fig. 8. A conceptual schematic of possible mechanism for electron transfer at microbial cell/GO interface leading to the production of RGO (OM: Outer membrane; IM: Inner membrane; mqn: menaquinone; $mqnH_2$: menaquinol; c-Cyts: c-type cytochromes).

Declaration of competing interest

The authors declare that they have no known competing financial interests or personal relationships that could have appeared to influence the work reported in this paper.

CRediT authorship contribution statement

Yue Lu: Conceptualization, Methodology, Resources, Formal analysis, Writing - original draft, Writing - review & editing. **Linrui Zhong:** Conceptualization, Methodology, Validation, Formal analysis, Investigation, Writing - original draft, Writing - review & editing. **Lin Tang:** Conceptualization, Resources, Writing - original draft. **Huan Wang:** Methodology, Writing - original draft. **Zhaohui Yang:** Methodology, Resources. **Qingqing Xie:** Writing - original draft, Writing - review & editing. **Haopeng Feng:** Writing - original draft. **Meiying Jia:** Writing - original draft. **Changzheng Fan:** Resources.

Acknowledgements

We thank the research group of Prof. Hanqing Yu (University of Science & Technology of China) to provide *Geobacter sulfurreducens* PCA.

This work was supported by the National Natural Science Foundation of China (Grant No. 51709100, 51679084, 51579096), the Fundamental Research Funds for the Central Universities (531107050936), the National Innovative Talent Promotion Program of China (2017RA 2088), and the Funds for Innovative Province Construction of Hunan Province of China (2019RS3012).

Appendix A. Supplementary data

Supplementary data to this article can be found online at https://doi.org/10.1016/j.chemosphere.2020.127141.

References

Afzali, M., Mostafavi, A., Shamspur, T., 2019. Designing an Au/reduced graphene oxide modified carbon paste electrode for the electrochemical quantification of agnuside. Sensor. Actuator. B Chem. 290, 188–194.

Akhavan, O., Ghaderi, E., 2012. *Escherichia coli* bacteria reduce graphene oxide to bactericidal graphene in a self-limiting manner. Carbon 50, 1853–1860.

Bansal, P., Doshi, S., Panwar, A.S., Bahadur, D., 2015. Exoelectrogens leading to precise reduction of graphene oxide by flexibly switching their environment during respiration. ACS Appl. Mater. Interfaces 7, 20576–20584.

Busalmen, J.P., Esteve-Nfflez, A., Berna, A., Feliu, J.M., 2008. C-type cytochromes wire electricity-producing bacteria to electrodes. Angew. Chem. Int. Ed. 47, 4874–4877.

Cai, X., Huang, L., Yang, G., Yu, Z., Wen, J., Zhou, S., 2018. Transcriptomic, proteomic, and bioelectrochemical characterization of an exoelectrogen *Geobacter* soli grown with different electron acceptors. Front. Microbiol. 9, 1075.

Cai, J., Gou, X., Sun, B., Li, W., Li, D., Liu, J., Hu, F., Li, Y., 2019. Porous graphene-black phosphorus nanocomposite modified electrode for detection of leptin. Biosens. Bioelectron. 137, 88–95.

Chen, J., Zhang, Y., Zhang, M., Yao, B., Li, Y., Huang, L., Li, C., Shi, G., 2016. Water-enhanced oxidation of graphite to graphene oxide with controlled species of oxygenated groups. Chem. Sci. 7, 1874–1881.

Chen, Z., Li, H., Ma, W., Fu, D., Han, K., Wang, H., He, N., Li, Q., Wang, Y., 2018. Addition of graphene sheets enhances reductive dissolution of arsenic and iron from arsenic contaminated soil. Land Degrad. Dev. 29, 572–584.

Cho, J.Y., Jang, J.I., Lee, W.K., Jeong, S.Y., Hwang, J.Y., Lee, H.S., Park, J.H., Jeong, S.Y., Jeong, H.J., Lee, G.W., Han, J.T., 2018. Fabrication of high-quality or highly porous graphene sheets from exfoliated graphene oxide via reactions in alkaline solutions. Carbon 138, 219–226.

Combarros, R.G., Collado, S., Diaz, M., 2016. Toxicity of graphene oxide on growth and metabolism of *Pseudomonas putida*. J. Hazard Mater. 310, 246–252.

Delgado, V.P., Paquete, C.M., Sturm, G., Gescher, J., 2019. Improvement of the electron transfer rate in *Shewanella oneidensis* MR-1 using a tailored periplasmic protein composition. Bioelectrochemistry 129, 18–25.

Feng, C., Deng, Y., Tang, L., Zeng, G., Wang, J., Yu, J., Liu, Y., Peng, B., Feng, H., Wang, J., 2018. Core-shell Ag_2CrO_4/N-GQDs@g-C_3N_4 composites with anti-photocorrosion performance for enhanced full-spectrum-light photocatalytic activities. Appl. Catal. B Environ. 239, 525–536.

Gurunathan, S., Han, J.W., Eppakayala, V., Kim, J.H., 2013. Microbial reduction of graphene oxide by *Escherichia coli*: a green chemistry approach. Colloid Surf. B-Biointerfaces 102, 772–777.

Hu, X., Zhou, Q., 2013. Health and ecosystem risks of graphene. Chem. Rev. 113, 3815–3835.

Hu, W., Peng, C., Luo, W., Lv, M., Li, X., Li, D., Huang, Q., Fan, C., 2010. Graphene-based antibacterial paper. ACS Nano 4, 4317–4323.

Huang, Y., Wei, Q., Wang, Y., Dai, L., 2018. Three-dimensional amine-terminated ionic liquid functionalized graphene/Pd composite aerogel as highly efficient and recyclable catalyst for the suzuki cross-coupling reactions. Carbon 136, 150–159.

Jiao, Y., Qian, F., Li, Y., Wang, G., Saltikov, C.W., Gralnick, J.A., 2011. Deciphering the electron transport pathway for graphene oxide reduction by *Shewanella oneidensis* MR-1. J. Bacteriol. 193, 3662–3665.

Kalathil, S., Katuri, K.P., Alazmi, A.S., Pedireddy, S., Kornienko, N., Costa, P.M.F.J., Saikaly, P.E., 2019. Bioinspired synthesis of reduced graphene oxide-wrapped *Geobacter sulfurreducens* as a hybrid electrocatalyst for efficient oxygen evolution reaction. Chem. Mater. 31, 3686–3693.

Karim, M.R., Hatakeyama, K., Matsui, T., Takehira, H., Taniguchi, T., Koinuma, M., Matsumoto, Y., Akutagawa, T., Nakamura, T., Noro, S.I., Yamada, T., Kitagawa, H., Hayami, S., 2013. Graphene oxide nanosheet with high proton conductivity. J. Am. Chem. Soc. 135, 8097–8100.

Kauffmanab, D.R., Star, A., 2010. Graphene versus carbon nanotubes for chemical sensor and fuel cell applications. Analyst 135, 2790–2797.

Li, D., Muller, M., Gilje, S., Kaner, R.B., Wallace, G.G., 2008a. Processable aqueous dispersions of graphene nanosheets. Nat. Nanotechnol. 3, 101–105.

Li, X.L., Wang, X.R., Zhang, L., Lee, S.W., Dai, H.J., 2008b. Chemically derived, ultra-smooth graphene nanoribbon semiconductors. Science 319, 1229–1232.

Li, D., Cheng, Y., Li, L., Li, W., Huang, Y., Pei, D., Tong, Z., Mu, Y., Yu, H., 2014. Light-driven microbial dissimilatory electron transfer to hematite. Phys. Chem. Chem. Phys. 16, 23003–23011.

Liu, Y., Zhang, F., Li, J., Li, D., Liu, D., Li, W., Yu, H., 2017. Exclusive extracellular bioreduction of methyl orange by azo reductase-free *Geobacter sulfurreducens*. Environ. Sci. Technol. 51, 8616–8623.

Logan, B.E., 2009. Exoelectrogenic bacteria that power microbial fuel cells. Nat. Rev. Microbiol. 7, 375–381.

Lovley, D.R., 2006. Bug juice: harvesting electricity with microorganisms. Nat. Rev. Microbiol. 4, 497–508.

Lovley, D.R., Giovannoni, S.J., White, D.C., Champine, J.E., Phillips, E.J.P., Gorby, Y.A., Goodwin, S., 1993. *Geobacter metallireducens* gen. nov. sp. nov., a microorganism capable of coupling the complete oxidation of organic compounds to the reduction of iron and other metals. Arch. Microbiol. 159, 336–344.

Luan, B., Huynh, T., Zhao, L., Zhou, R., 2015. Potential toxicity of graphene to cell functions via disrupting protein-protein interactions. ACS Nano 9, 663–669.

Mahadevan, R., Bond, D.R., Butler, J.E., Esteve-Nunez, A., Coppi, M.V., Palsson, B.O., Schilling, C.H., Lovley, D.R., 2006. Characterization of metabolism in the Fe(iii)-reducing organism *Geobacter sulfurreducens* by constraint-based modeling. Appl. Environ. Microbiol. 72, 1558–1568.

Malvankar, N.S., Vargas, M., Nevin, K.P., Franks, A.E., Leang, C., Kim, B.C., Inoue, K., Mester, T., Covalla, S.F., Johnson, J.P., Rotello, V.M., Tuominen, M.T., Lovley, D.R., 2011. Tunable metallic-like conductivity in microbial nanowire networks. Nat. Nanotechnol. 6, 573–579.

Meng, J., Xu, Z., Guo, J., Yue, Y., Sun, X., 2013. Analysis of enhanced current-generating mechanism of *Geobacter sulfurreducens* strain via model-driven metabolism simulation. PloS One 8, e73907.

Michelson, K., Sanford, R.A., Valocchi, A.J., Werth, C.J., 2017. Nanowires of *Geobacter sulfurreducens* require redox cofactors to reduce metals in pore spaces too small for cell passage. Environ. Sci. Technol. 51, 11660–11668.

Mohanty, N., Berry, V., 2008. Graphene-based single-bacterium resolution biodevice and DNA transistor: interfacing graphene derivatives with nanoscale and microscale biocomponents. Nano Lett. 8, 4469–4476.

Mokkapati, V.R.S.S., Pandit, S., Kim, J., Martensson, A., Lovmar, M., Westerlund, F., Mijakovic, I., 2018. Bacterial response to graphene oxide and reduced graphene oxide integrated in agar plates. R. Soc. Open Sci. 5, 181083.

Okamoto, A., Saito, K., Inoue, K., Nealson, K.H., Hashimoto, K., Nakamura, R., 2014. Uptake of self-secreted flavins as bound cofactors for extracellular electron transfer in *Geobacter* species. Energy Environ. Sci. 7, 1357–1361.

Pei, S., Cheng, H.M., 2012. The reduction of graphene oxide. Carbon 50, 3210–3328.

Peng, L., Zhang, Y., 2017. Cytochrome OmcZ is essential for the current generation by *Geobacter sulfurreducens* under low electrode potential. Electrochim. Acta 228, 447–452.

Peng, B., Tang, L., Zeng, G., Fang, S., Ouyang, X., Long, B., Zhou, Y., Deng, Y., Liu, Y., Wang, J., 2018. Self-powered photoelectrochemical aptasensor based on phosphorus doped porous ultrathin g-C_3N_4 nanosheets enhanced by surface plasmon resonance effect. Biosens. Bioelectron. 121, 19–26.

Prakash, A., Bahadur, D., 2014. The role of ionic electrolytes on capacitive performance of ZnO-reduced graphene oxide nanohybrids with thermally tunable morphologies. ACS Appl. Mater. Interfaces 6, 1394–1405.

Manasi, Rajesh, V., Rajesh, N., 2018. Biosorption study of cadmium, lead and zinc ions onto halophilic bacteria and reduced graphene oxide. J. Environ. Chem. Eng 6, 5053–5060.

Rajpurohit, A.S., Punde, N.S., Rawool, C.R., Srivastava, A.K., 2019. Fabrication of high energy density symmetric supercapacitor based on cobalt-nickel bimetallic tungstate nanoparticles decorated phosphorus-sulphur co-doped graphene nanosheets with extended voltage. Chem. Eng. J. 371, 679–692.

Rathinam, N.K., Berchmans, S., Sani, R.K., Salem, D.R., 2018. Rewiring the microbe-electrode interfaces with biologically reduced graphene oxide for improved bioelectrocatalysis. Bioresour. Technol. 256, 195–200.

Reich, S., Thomsen, C., 2004. Raman spectroscopy of graphite. Phil. Trans. Roy. Soc. Lond. 362, 2271–2288.

Ren, X., Zeng, G., Tang, L., Wang, J., Wan, J., Feng, H., Song, B., Huang, C., Tang, X., 2018. Effect of exogenous carbonaceous materials on the bioavailability of organic pollutants and their ecological risks. Soil Biol. Biochem. 116, 70–81.

Richter, H., Nevin, K.P., Jia, H.F., Lowy, D.A., Lovley, D.R., Tender, L.M., 2009. Cyclic voltammetry of biofilms of wild type and mutant *Geobacter sulfurreducens* on fuel cell anodes indicates possible roles of OmcB, OmcZ, type IV pili, and protons in extracellular electron transfer. Energy Environ. Sci. 2, 506–516.

Rostamabadi, P.F., Heydari-Bafrooei, E., 2019. Impedimetric aptasensing of the breast cancer biomarker HER2 using a glassy carbon electrode modified with gold nanoparticles in a composite consisting of electrochemically reduced graphene oxide and single-walled carbon canotubes. Microchim. Acta 186, 495.

Salas, E.C., Sun, Z.Z., Luttge, A., Tour, J.M., 2010. Reduction of graphene oxide via bacterial respiration. ACS Nano 4, 4852–4856.

Shen, L., Jin, Z., Wang, D., Wang, Y., Lu, Y., 2018. Enhance wastewater biological treatment through the bacteria induced graphene oxide hydrogel. Chemosphere 190, 201–210.

Song, J., Sasaki, D., Sasaki, K., Kato, S., Kondo, A., Hashimoto, K., Nakanishi, S., 2016. Comprehensive metabolomic analyses of anode-respiring *Geobacter sulfurreducens* cells: the impact of anode-respiration activity on intracellular metabolite levels. Process Biochem. 51, 34–38.

Srivastava, M., Tiwari, P., Mall, V.K., Srivastava, S.K., Prakash, R., 2019. Voltammetric determination of the antimalarial drug chloroquine using a glassy carbon electrode modified with reduced graphene oxide on WS_2 quantum dots. Microchim. Acta 186, 415.

Stankovich, S., Dikin, D.A., Piner, R.D., Kohlhaas, K.A., Kleinhammes, A., Jia, Y.Y., Wu, Y., Nguyen, S.T., Ruoff, R.S., 2007. Synthesis of graphene-based nanosheets via chemical reduction of exfoliated graphite oxide. Carbon 45, 1558–1565.

Tang, L., Feng, C., Deng, Y., Zeng, G., Wang, J., Liu, Y., Feng, H., Wang, J., 2018a. Enhanced photocatalytic activity of ternary Ag/g-C_3N_4/$NaTaO_3$ photocatalysts under wide spectrum light radiation: the high potential band protection mechanism. Appl. Catal. B Environ. 230, 102–114.

Tang, L., Liu, Y., Wang, J., Zeng, G., Deng, Y., Dong, H., Feng, H., Wang, J., Peng, B., 2018b. Enhanced activation process of persulfate by mesoporous carbon for degradation of aqueous organic pollutants: electron transfer mechanism. Appl. Catal. B Environ. 231, 1–10.

Wang, Z.J., Zhou, X.Z., Zhang, J., Boey, F., Zhang, H., 2009. Direct electrochemical reduction of single-layer graphene oxide and subsequent functionalization with *Glucose Oxidase*. J. Phys. Chem. C 113, 14071–14075.
Wang, G., Qian, F., Saltikov, C., Jiao, Y., Li, Y., 2011. Microbial reduction of graphene oxide by *Shewanella*. Nano Res. 4, 563–570.
Wang, Z., Xu, D., Huang, Y., Wu, Z., Wang, L., Zhang, X., 2012. Facile, mild and fast thermal-decomposition reduction of graphene oxide in air and its application in high-performance lithium batteries. Chem. Commun. 48, 976–978.
Wang, F., Dong, X., Wang, K., Duan, W., Gao, M., Zhai, Z., Zhu, C., Wang, W., 2019a. Laser-induced nitrogen-doped hierarchically porous graphene for advanced electrochemical energy storage. Carbon 150, 396–407.
Wang, X., Zhu, Y., Chen, M., Yan, M., Zeng, G., Huang, D., 2019b. How do proteins 'response' to common carbon nanomaterials? Adv. Colloid Interface Sci. 270, 101–107.
Wei, J., Hu, Y., Liang, Y., Kong, B., Zhang, J., Song, J., Bao, Q., Simon, G., Jiang, S., Wang, H., 2015. Nitrogen-doped nanoporous carbon/graphene nanosandwiches: synthesis and application for efficient oxygen reduction. Adv. Funct. Mater. 25, 5768–5777.
Williams, G., Kamat, P.V., 2009. Graphene-semiconductor nanocomposites: excited-state interactions between ZnO nanoparticles and graphene oxide. Langmuir 25, 13869–13873.
Xu, L.Q., Liu, Y.L., Neoh, K.G., Kang, E.T., Fu, G.D., 2011. Reduction of graphene oxide by aniline with its concomitant oxidative polymerization. Macromol. Rapid Commun. 32, 684–688.
Yoshida, N., Miyata, Y., Doi, K., Goto, Y., Nagao, Y., Tero, R., Hiraishi, A., 2016. Graphene oxide-dependent growth and self-aggregation into a hydrogel complex of exoelectrogenic bacteria. Sci. Rep. 6, 21867.
You, L., Liu, L., Xiao, Y., Dai, Y., Chen, B., Jiang, Y., Zhao, F., 2018. Flavins mediate extracellular electron transfer in gram-positive *Bacillus megaterium* strain LLD-1. Bioelectrochemistry 119, 196–202.
Zhao, H., Zhang, C., Wang, Y., Chen, W., Alvarez, P.J.J., 2018. Self-damaging aerobic reduction of graphene oxide by *Escherichia coli*: role of go-mediated extracellular superoxide formation. Environ. Sci. Technol. 52, 12783–12791.
Zhou, M., Wang, Y.L., Zhai, Y.M., Zhai, J.F., Ren, W., Wang, F., Dong, S.J., 2009. Controlled synthesis of large-area and patterned electrochemically reduced graphene oxide films. Chem. Eur J. 15, 6116–6120.
Zhou, S., Lin, M., Zhuang, Z., Liu, P., Chen, Z., 2019. Biosynthetic graphene enhanced extracellular electron transfer for high performance anode in microbial fuel cell. Chemosphere 232, 396–402.